

Quantum illumination using non-Gaussian states with conditional measurementsHuan Zhang,¹ Ying Xia,¹ Wei Ye,² Shoukang Chang³,^{*} and Zeyang Liao^{1,*}¹State Key Laboratory of Optoelectronic Materials and Technologies, School of Physics, Sun Yat-sen University, Guangzhou 510275, China²School of Information Engineering, Nanchang Hangkong University, Nanchang 330063, China³MOE Key Laboratory for Nonequilibrium Synthesis and Modulation of Condensed Matter, Shaanxi Province Key Laboratory of Quantum Information and Quantum Optoelectronic Devices, School of Physics, Xi'an Jiaotong University, 710049, People's Republic of China

(Received 3 April 2024; accepted 11 June 2024; published 28 June 2024)

Quantum illumination is a quantum sensing protocol primarily used for object detection, which aims to detect the presence of a target with low reflectivity in the free space using quantum light fields. Here we investigate a quantum illumination scheme using an entangled light source by performing non-Gaussian operations on the two-mode squeezed vacuum (TMSV) state in order to reduce the detection error probability and meanwhile improve the signal-to-noise (SNR) ratio. We demonstrate that under the same squeezing parameter, the non-Gaussian operations can significantly reduce the detection error rate compared with the original TMSV state. Under the same average signal photon number, both the TMSV states with and without non-Gaussian operations can provide smaller error rate than that of the coherent state. In addition, we consider the balanced homodyne detection on idler and return signal photons as joint measurement and find that non-Gaussian operations can enhance the SNR of target detection by about 6–9 dB compared with that using TMSV. These results here demonstrate the advantage of the non-Gaussian entangled source in quantum illumination protocol and can find potential applications in target detection in noisy environment.

DOI: [10.1103/PhysRevA.109.062440](https://doi.org/10.1103/PhysRevA.109.062440)**I. INTRODUCTION**

Quantum entanglement, one of the most important quantum resources, has found important applications in the areas such as quantum computation [1–3], quantum communication [4–6], and quantum sensing [7–10]. Quantum target perception and detection protocol, also known as quantum illumination protocol (QI), as an important subset in the field of quantum sensing, aims to accurately distinguish between the presence and absence of target with extremely low reflectivity in a distant region [11–14]. In a typical QI protocol, we first prepare entangled light sources with one mode of the radiation source (signal) being sent to the region where the target may exist, while the other mode is stored locally as an idler to perform the joint quantum measurement with the signal light reflected by the target. In the QI protocol, the precision limit of the joint quantum measurement is given by the quantum Chernoff bound (QCB), which is an upper bound of the error probability of the hypothesis test problem [15,16]. The previous studies have shown that quantum entanglement is a critical resource for enhancing the performance of target detection, even if entanglement is disrupted by the noisy environments [17,18].

Lloyd first proposed the QI protocol based on the discrete variable quantum states such as the entangled single-photon sources and showed how to identify the existence of weak reflective target even in noisy environments [11]. In 2021, Xu *et al.* experimentally demonstrated the advantage of the QI

by using polarization-entangled photon pairs and showed that the QI can surpass the classical limit by up to 40% [19]. The optimal probe state for minimizing the error probability of the QI using discrete variable quantum states has been determined [20]. In addition to discrete variable quantum states, the QI scheme was also extended to continuous-variable states, such as the Gaussian state, by Tan *et al.* [12]. They showed that the performance of the QI system based on the Gaussian entangled state is better than that of the optimal classical illumination system using a coherent state for the same transmission energy in a bright noise environment. The advantages of the QI based on the Gaussian entangled states have also been experimentally demonstrated [21–23]. However, the QI using Gaussian entangled states is not the optimal choice in the continuous-variable region [24]. A number of schemes have been proposed to further improve the performance of the QI via enhancing the entanglement of radiation sources [25–28]. It has been shown that by performing non-Gaussian operations such as photon addition (PA), photon subtraction (PS), and photon catalysis (PC), the entanglement of Gaussian entangled states can be further enhanced [29–35] and can be used to improve the performance of continuous-variable quantum key distribution [36,37], quantum precision metrology [38,39], and QI [27,28]. Zhang *et al.* have shown that the photon subtracted from the two-mode squeezed vacuum state (TMSV) has a lower error probability compared to the original the TMSV at the same squeezing intensity [27]. Fan *et al.* proposed that by performing the photon addition or the coherent superposition of photon addition and subtraction operations on both two modes of the TMSV, the performance of the QI can be improved [28]. In these studies, they

*Contact author: liaozy7@mail.sysu.edu.cn

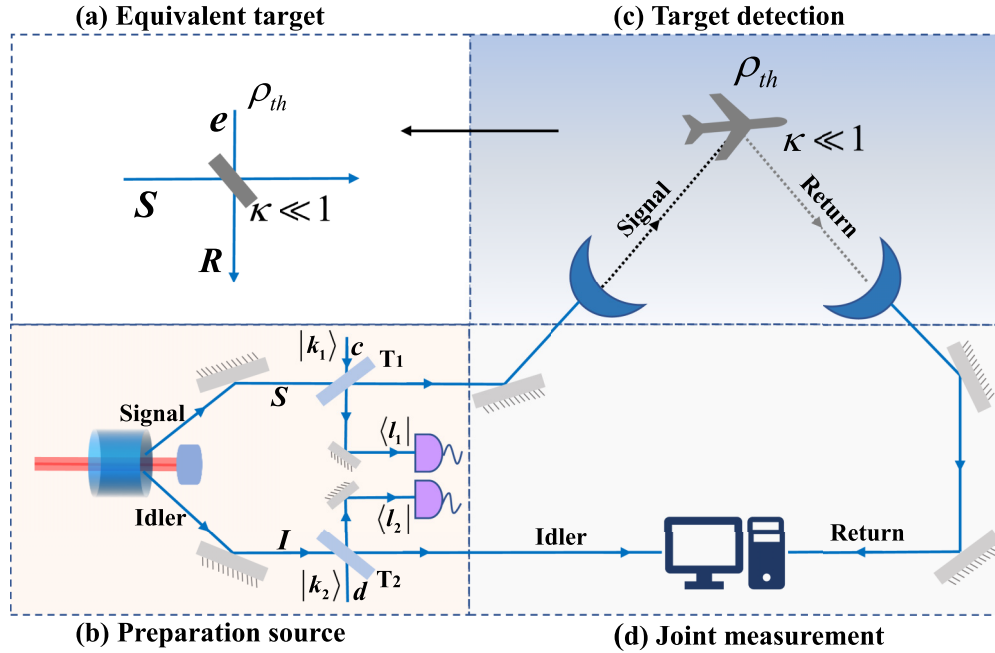


FIG. 1. Schematic diagrams of QI protocol based on non-Gaussian entangled states. (a) The target can be modeled as an optical beam splitter with the extreme low reflectivity $\kappa \ll 1$. The execution of the QI protocol is divided into three steps. (b) Step 1: source preparation: performing non-Gaussian operations based on conditional measurement on the initial Gaussian entangled state that can be obtained by an optical parametric amplifier with the pump field, resulting in non-Gaussian entangled state with enhanced entanglement. (c) Step 2: target detection: emitting signal light to illuminate the potential region of the target, and if the target is present, the signal light can be reflected. (d) Step 3: joint measurement: after receiving photons from the target region, a joint quantum measurement is performed on the return and the idler lights.

mainly considered the ideal non-Gaussian operations without considering their practical realizations. Additionally, what kind of joint quantum measurement is needed to demonstrate the advantage of the non-Gaussian quantum states is also missing.

Considering that quantum entanglement can be enhanced by performing non-Gaussian operation based on conditional measurement (NGOCM) on the TMSV [40–44], in this paper we propose a QI scheme which uses the NGOCM-TMSV quantum light sources to improve the performance of the target detection. The advantage of this scheme is that we can use an optical beam splitter to simulate three different non-Gaussian operations simultaneously, including PA, PS, and PC operations. The results show that a lower error probability can be achieved by using all three non-Gaussian operations. In addition, we implement the joint quantum measurement for the returned and idler light using balanced homodyne detection. The results show that the three non-Gaussian operations can enhance the signal-to-noise ratio (SNR) of target detection by approximately 6–9 dB. Our results here can find applications in the target detection with noisy environment.

The structure of the paper is as follows. In Sec. II, we introduce the non-Gaussian entangled sources based on the NGOCM. The performance of the QI is analyzed in Sec. III. In Sec. III A, we analyze the error probability of the QI, and in Sec. III B, we implement the joint quantum measurement for the returned and idler light by using the balanced homodyne detection, and analyzes the SNR. Our results are summarized in Sec. IV.

II. PREPARATION OF THE NON-GAUSSIAN ENTANGLED SOURCES

The task of QI is to discover an unknown target with extremely low reflectivity in free space, where the thermal noise is present, as shown in Fig. 1. In entanglement-based QI protocols, the precise detection of the target hidden in the background can be divided into three steps: (1) Preparation and optimization of quantum state with large entanglement [Fig. 1(b)]; (2) illuminating the potential region of the target by emitting signal light [Fig. 1(c)]; (3) enforcement of joint quantum measurement on the return and idler lights after receiving photons from the region [Fig. 1(d)]. In this section, we investigate the preparation and optimization of entanglement sources by using the NGOCM in the QI system.

In our scheme, we first employ an optical parametric amplifier with the pump field to obtain the signal and idler mode pair [45,46], i.e., the two-mode squeezed vacuum (TMSV) state

$$|\psi\rangle_{SI} = \sqrt{1 - \lambda^2} \sum_{n=0}^{\infty} \lambda^n |n\rangle_S |n\rangle_I, \quad (1)$$

where $\lambda = \tanh r$ with r being the squeezing parameter. The subscripts S and I denote signal and idler modes. In Ref. [12], the QI has been realized using the TMSV as the entangled source, demonstrating a 6-dB advantage in the error-probability exponent over the optimum reception coherent-state system. The results show that entanglement is a key quantum resource for improving the performance of QI. Since quantum entanglement may be further enhanced by

performing non-Gaussian operation on TMSV, here we consider to use the TMSV light source with NGOCM to reduce the error probability in the QI.

In Fig. 1(b), we first employ the NGOCM on each mode of the TMSV, where we denote two ancillary inputs as modes c and d . In the NGOCM, the signal light source and an ancillary Fock state with k_i photon ($i = 1, 2$) are injected from two ports of the beam splitter BS (T_i) with transmissivity $T_i = \cos^2 \theta$ ($i = 1, 2$), and then projective measurement is performed on the ancillary path where l_i photon ($i = 1, 2$) Fock state is obtained with certain probability. The BS transmissivity T_i is an important parameter which is relevant to the success probability of the non-Gaussian operation.

We here mainly consider three different NGOCMs with single-photon input: single-photon subtraction (PS) with $(k_i, l_i) = (0, 1)$, single-photon addition (PA) with $(k_i, l_i) = (1, 0)$, and single-photon catalysis (PC) with $(k_i, l_i) = (1, 1)$. For the double-side NGOCMs, we can obtain

$$|\psi\rangle_{SI}^{n-G} = \sum_{n=0}^{\infty} c_n |n\rangle_S |n\rangle_I, \quad (2)$$

where c_n is the normalized coefficient of the Schmidt decomposition and its values for the three NGOCMs, including PA, PS, and PC, are provided in Appendix A.

To demonstrate that a lower error probability can be obtained by increasing entanglement of the emission sources, we first discuss the entanglement properties of the non-Gaussian entangled states by using the von Neumann entropy. For any pure state in the Schmidt form as shown in Eq. (2), the entanglement can be quantified by the partial von Neumann entropy of the reduced density operator [47], i.e., $E(|\psi\rangle_{SI}) = -\text{Tr}(\rho_S \log_2 \rho_S)$ where $\rho_S = \text{Tr}_I(|\psi\rangle_{SI}\langle\psi|)$. On substituting Eq. (2), we can obtain

$$E(|\psi\rangle_{SI}^{n-G}) = -\sum_{n=0}^{\infty} c_n^2 \log_2 c_n^2 \quad (3)$$

for the non-Gaussian entangled states. In particular, for the TMSV, the degree of entanglement can be calculated as $E(|\psi\rangle_{SI}) = \cosh^2 r \log_2 \cosh^2 r - \sinh^2 r \log_2 \sinh^2 r$, which is the benchmark for measuring the improvement in entanglement using the NGOCM operations [48]. If $E(|\psi\rangle_{SI}^{n-G}) > E(|\psi\rangle_{SI})$, the entanglement is enhanced by the NGOCM. Otherwise, the entanglement is reduced by the NGOCM.

In Fig. 2, we plot the enhancement amount of the von Neumann entropy $r_E = [E(|\psi\rangle_{SI}^{n-G}) - E(|\psi\rangle_{SI})]/E(|\psi\rangle_{SI})$ as a function of transmissivity T_1 and T_2 . The result for the PC operation is shown in Fig. 2(a), from which we can see that there are actually three enhanced regions for the entanglement compared with that of the TMSV. One enhanced region is located in the low transmissivities of two BSs, while the other two are located in one-small-one-large transmissivity of two BSs. When $T_1, T_2 \rightarrow 1$, the signal and idler photons are not affected by the beam splitters and the results should be the same as the TMSV. Indeed, the enhancement of entanglement $r_E = 0$ when $T_1 = T_2 = 1$ as shown in Fig. 2. On the contrary, for PA and PS operations, the enhanced regions of the entanglement are the same and they are located in the region with high transmissivities of both two BSs as shown in Fig. 2(b). It is seen that the enhancement of quantum entanglement is

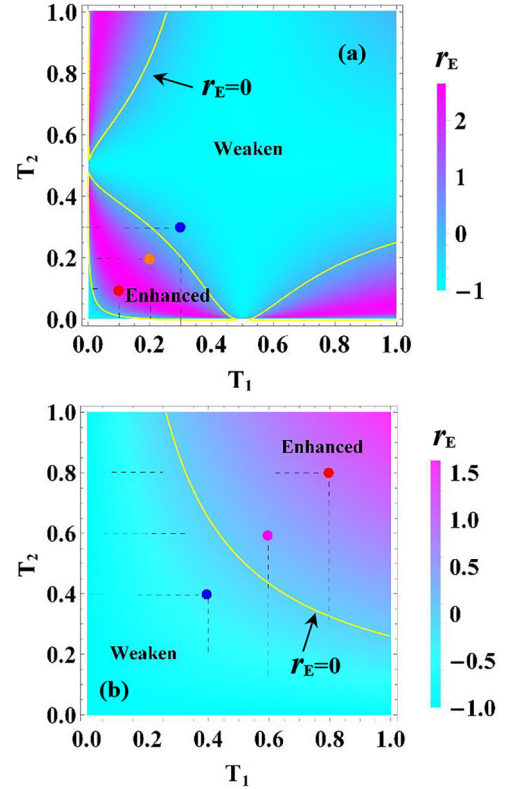


FIG. 2. The enhancement ratio of the von Neumann entropy r_E as a function of the transmissivity T_1 and T_2 of the NGOCM operations for the PC operation (a) and for the PA and PS operations (b). The red and magenta dots correspond to two points where the quantum entanglement is enhanced, while the blue dot is not. The error probabilities of target detection corresponding to these three data points are discussed in the main text. The squeezing parameter of the incident TMSV source is fixed to be $\sinh^2(r) = 0.05$.

the largest when $T_1, T_2 \rightarrow 1$ for the PA and PS operations. However, we should note that when $T_1, T_2 \rightarrow 1$, the success probability for the PA and PS operations vanishes because the beam splitters become transparent and no photon addition or subtraction can be performed. Thus, by performing NGOCM with suitable parameters on the TMSV, we can increase the entanglement of the light source. To investigate the relationship between quantum entanglement and the error probability of QI, we take three data points located in regions with and without improved entanglement, as shown in Fig. 2. We will discuss the error probability of target detection in the next section based on these data points.

III. PERFORMANCE ANALYSIS OF QUANTUM ILLUMINATION

A. Error probability

In this subsection, we first introduce the basic theoretical analysis of the QI protocol, as illustrated in Fig. 1. The signal light from the entangled source which is discussed in the previous section is emitted into the region where the target may exist, aiming to identify it amidst the noise background. Here we set \hat{a}_S , \hat{a}_I , and \hat{a}_e as the field annihilation operators corresponding to the signal mode, the idler mode, and the

environment thermal noise mode, respectively. Mathematically, the target can be modeled as a beam splitter $\text{BS}(\kappa)$ with the reflectivity $\kappa \ll 1$ [see Fig. 1(a)]. When the target is absent, we have $\kappa = 0$, all the environment thermal states in noise mode e will be injected into the joint quantum measurement device shown in Fig. 1(d). In this case, the final quantum state before the joined quantum measurement is given by

$$\rho_{\text{SI}}^{(0)} = \text{Tr}_S[\rho_{\text{SI}}^{\text{n-G}}] \otimes \rho_{\text{th}}(N_e), \quad (4)$$

where $\rho_{\text{SI}}^{\text{n-G}}$ can be obtained by Eq. (2) and $\rho_{\text{th}}(N_e) = \sum_{m=0}^{\infty} \frac{1}{N_e+1} \left(\frac{N_e}{N_e+1}\right)^m |m\rangle\langle m|$ is the thermal noise in surrounding region of the object with the average photon number N_e .

On the other hand, if an object is present, the signal light may be reflected by the object and the returning light source is a mixture of signal light and environment thermal noise. This process can be modeled as a beam splitter $\text{BS}(\kappa)$ with a two-mode mixing operator

$$\text{BS}(\kappa) = \exp\left\{\arctan\left(\sqrt{\frac{\kappa}{1-\kappa}}\right)(\hat{a}_S \hat{a}_e^\dagger - \hat{a}_S^\dagger \hat{a}_e)\right\}. \quad (5)$$

In this case, the final quantum state before the joined quantum measurement is given by

$$\rho_{\text{SI}}^{(1)} = \text{Tr}_e[\text{BS}(\kappa)\rho_{\text{SI}}^{\text{n-G}} \otimes \rho_{\text{th}}(N'_e)\text{BS}^\dagger(\kappa)]. \quad (6)$$

It should be noted that, in this case, the average photon number of thermal noise is adjusted to $N'_e = N_e/(1-\kappa)$ to compensate for the loss during mixing. Finally, a joint quantum measurement is performed on the returning and idler light to distinguish between the case where the target does not exist $\rho_{\text{SI}}^{(0)}$ and the case where the target exists $\rho_{\text{SI}}^{(1)}$.

To see the advantages of non-Gaussian entangled states for the QI more clearly, we assume to use a positive operator-valued measurement (POVM) as the joint quantum measurement scheme to infer whether an object is present or not. The precision of target recognition can be judged by the inferred error probability, which also depends on a prior probability. Here, we assume a prior probability of $\frac{1}{2}$, meaning that the two hypotheses, whether the region contains a target or not, are equally likely. Then, the minimal error probability with a joint state of K -copy entanglement is given by the Helstrom limit [11,12,49]

$$P_{\text{err}} = \frac{1}{2} \left(1 - \frac{1}{2} \|\rho_{\text{SI}}^{(1)\otimes K} - \rho_{\text{SI}}^{(0)\otimes K}\|\right), \quad (7)$$

where the symbol $\|\Theta\|$ is the trace norm, i.e., $\|\Theta\| = \text{Tr}[\sqrt{\Theta^\dagger \Theta}]$ which is the sum of the singular values of Θ . Thus, larger trace distance between $\rho_{\text{SI}}^{(0)}$ and $\rho_{\text{SI}}^{(1)}$ will give smaller P_{err} . However, as known to us, the continuous-variable non-Gaussian state [e.g., $\rho_{\text{SI}}^{\text{n-G}}$ in Eq. (4)] is actually a superposition of an infinite-dimensional Fock state in Hilbert space. In addition, to achieve quantum advantages, we will need a very large K -copy entanglement. These undoubtedly make it difficult for us to directly evaluate the probability of errors P_{err} by using Eq. (7). At this point, the quantum Chernoff bound (QCB) comes to a rescue, which can help us to solve this problem. For optimum quantum discrimination between a pair of equally likely K -copy entangled states, $\rho_{\text{SI}}^{(0)\otimes K}$ and $\rho_{\text{SI}}^{(1)\otimes K}$, the QCB places the following limit on the error

probability [15,16]:

$$P_{\text{err}} \leq \frac{1}{2} \left\{ \min_{0 \leq \tau \leq 1} \text{Tr} [(\rho_{\text{SI}}^{(0)})^\tau (\rho_{\text{SI}}^{(1)})^{(1-\tau)}] \right\}^K. \quad (8)$$

This bound is exponentially tight. We can evaluate the performance of the QI by using Eq. (8). However, notice that the QCB involves a minimization in the variable τ , which requires higher computational strategies and resources. Therefore, we set $\tau = \frac{1}{2}$, a weaker version of the Eq. (8), which is also known as the Bhattacharyya bound [12,50]:

$$P_{\text{err}} \leq P_{\text{err}}^B = \frac{1}{2} \left\{ \text{Tr} [(\rho_{\text{SI}}^{(0)})^{1/2} (\rho_{\text{SI}}^{(1)})^{1/2}] \right\}^K. \quad (9)$$

In the following, we compare the improvement of the QI performance among various NGOCMs by using Eq. (9) in the same dimension.

As is known, the TMSV is a zero-mean Gaussian state in the quadrature representation, which can be described with a covariance matrix in phase space [12]. Therefore, the formalism in Ref. [12] applies solely to a Gaussian state. When it comes to non-Gaussian states, we cannot obtain the error probability of target detection using the same method as for the TMSV. Fortunately, the non-Gaussian entangled states can be expanded with infinite-dimensional Fock states in the Hilbert space, as shown in Eq. (2), which provides a powerful and straightforward method for us to analyze QI in the non-Gaussian regime.

Substituting Eqs. (4) and (6) into Eq. (9), we can immediately evaluate the Bhattacharyya bound of the error probability via numerical methods. However, we cannot run and calculate the density operator in an infinite-dimensional Hilbert space and need to truncate the density operator to the quantum state with appropriate photon numbers. In the following numerical calculation, for the convenience of discussion and analysis, we truncate the photon numbers containing all non-Gaussian entangled states ($\rho_{\text{SI}}^{\text{n-G}}$) to $n_{\text{max}} = 15$ and neglect all the contributions of higher photon number, which is already a very good approximation when the initial entanglement source brightness is relatively weak ($N_s = \sinh^2 r = 0.05$ in this scheme). The Bhattacharyya bound can then be determined directly from the truncated density operators. Meanwhile, unless otherwise stated, all calculations presented in this work assume an average photon number of $N_e = 1$ for the thermal noise surrounding the target. This assumption represents a particularly strong level of thermal noise in free space. In addition, we choose target reflectivity to be $\kappa = 0.01$, i.e., assuming that only 1% of the signal light is reflected by the target to the detector. The transmissivity of the NGOCM devices is set to $T_1 = T_2 = T$.

In Fig. 3 the Bhattacharyya bound of the error probability P_{err}^B is plotted as a function of number of copies K . In these comparisons, we fix the squeezing parameter of the TMSV before non-Gaussian operations such that $\sinh^2(r) = 0.05$ and compare their error probabilities. For comparison, we also plot the error probability curve using the coherent state with the same average photon number as that of the TMSV. The advantage afforded by the NGOCMs can be clearly observed by showing the dependence of P_{err}^B on the number of copies K . For the PC operators, in Fig. 3(a), we provide the error probability corresponding to the three data points in Fig. 2(a), in which red ($T = 0.1$) and magenta ($T = 0.2$) data points

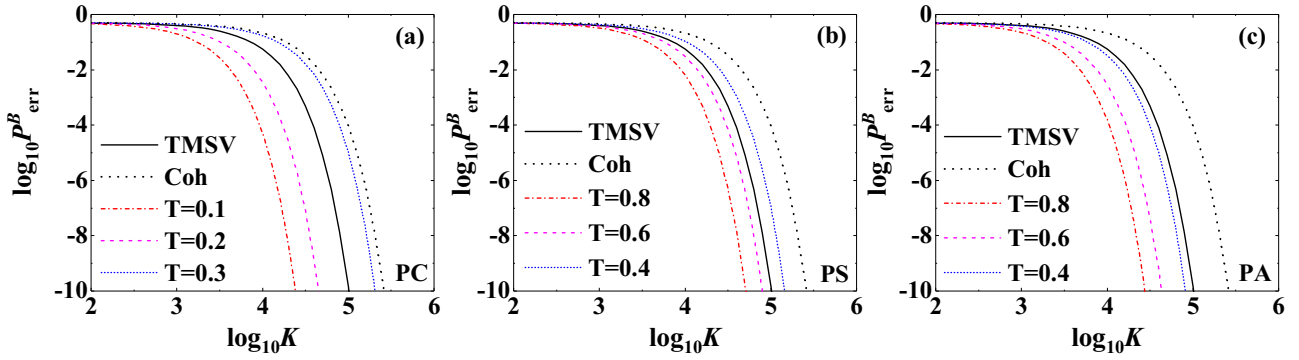


FIG. 3. Error probability of the target detection as a function of number of copies K by performing the PC operations with the transmissivity $T = (0.1, 0.2, 0.3)$ (a), the PS operations with $T = (0.8, 0.6, 0.4)$ (b), and the PA operations with $T = (0.8, 0.6, 0.4)$ (c) on the initial TMSV source. The error probability of the TMSV (black solid line) and coherent state (black dotted line) are also shown as benchmark for comparison. The reflectivity of the target is chosen as $\kappa = 0.01$. The squeezing parameter of the incident TMSV source is fixed to be $\sinh^2(r) = 0.05$. The thermal noise intensity is $N_e = 1$.

correspond to an increase in entanglement, while the blue ($T = 0.3$) data point does not. From Fig. 3(a), it is not difficult to find that performing the PC operations on each mode of the TMSV can significantly reduce the error probability in target detection with the same number of copies K , especially when K is large (e.g., $K \geq 10^4$). This improvement can be attributed to the enhancement of entanglement. It is worth mentioning that the success probabilities in the enhancement regions of entanglement are relatively low. In addition, the PC operation maximizes entanglement at low but nonzero probability. Thus, the success of detecting the single photon, also the key of the PC, is determined by the perfection of the detectors. As long as the detector is perfect enough, the single photon can be successfully detected. With current detection technology, it is possible to solve the issue of low detection probability. Furthermore, even if the single photon in the auxiliary mode is not detected, our scheme can still achieve the quantum advantage in target detection. The main reasons are as follows: on the one hand, to achieve quantum advantage here, we must ensure that $K \gg 1$, which can actually compensate for the low probability of success. That is to say, a portion of the multicopy TMSV states are always converted to PC-TMSV, thereby obtaining quantum advantages. On the other hand, if a single photon is not detected in auxiliary mode but a vacuum output is detected, then this operation actually transitions to PA operation. On the contrary, if the photon numbers $l_i > 1$ are detected in the auxiliary mode, then this situation shifts to PS operation. In fact, for both the PS and PA operations, by adjusting the transmissivity T of the BS(T_i) in the region of entanglement enhancement, the error probability can still be significantly reduced, as shown in Figs. 3(b) and 3(c). Even in areas where entanglement has not improved, the error probability of target detection obtained using PC and PS operations is still lower than that of coherent states.

In addition, for the PA operation, we are surprised to find that even if the entanglement is not enhanced, the PA operation can still reduce the error probability for target detection, as shown by the blue dotted line in Fig. 3(c). To explain this phenomenon, in Fig. 4(a), we show the signal intensity after performing the NGOCMs on TMSV, namely, the average photon numbers $\langle n \rangle_{\text{signal}}$ in the signal mode. We can observe

that the reduction of the error probability for the PA operation is mainly due to the fact that the PA operation can significantly increase the average photon numbers in the signal mode. From this, it can be seen that the reduction of error probability in target detection can be achieved by increasing the entanglement of the signal source and enhancing the signal intensity. In Fig. 4(b), we compare the error probability using coherent state, TMSV, PC- and PS-TMSV with the same average signal photon number (i.e., $N_s = 0.05$). Since the average photon number of PA-TMSV is larger than 1 as shown in Fig. 4(a), its error probability is not plotted in the figure. We can see that with the same average signal photon number, the error probabilities using TMSV, PC- and PS-TMSV are lower than that using the coherent state and in this case the TMSV input has the best performance.

In order to compare the QI performance of the entangled sources after performing different NGOCMs, in Figs. 5(a) and 5(b), we show the typical behavior of the von Neumann entropy E_v as a function of transmissivity T for the double-side and the single-side NGOCMs, respectively. From Fig. 5(a), we can easily find that when $T = 0.125$, the maximum entanglement $E_{v,\text{max}}^{\text{PC}} = 1.06$ for the double-side PC operation. While for the double-side PA and PS operations, the maximum entanglement $E_{v,\text{max}}^{\text{PA}} = E_{v,\text{max}}^{\text{PS}} = 0.763$ when $T \rightarrow 1$. In fact, the transmissivity $T \rightarrow 1$ can be used to realize ideal PA and PS operations, i.e., $|\psi\rangle_{\text{PA}} \rightarrow \hat{a}_S^\dagger \hat{a}_I^\dagger |\psi\rangle_{\text{SI}}$ and $|\psi\rangle_{\text{PS}} \rightarrow \hat{a}_S \hat{a}_I |\psi\rangle_{\text{SI}}$ for performing the PA and the PS operators on each mode of the TMSV, respectively. The ideal PA- and PS-TMSV has been compared with the TMSV for the QI [27,28]. Besides, from Fig. 5(b), we can obtain that the maximum entanglement $E_{v,\text{max}}^{\text{PC}} = 1.034$ when $T = 0.041$ for the single-side PC operation, which is slightly smaller than that of the double-side operations. For the single-side PA and PS operations, the maximum entanglement $E_{v,\text{max}}^{\text{PA}} = E_{v,\text{max}}^{\text{PS}} = 0.483$ also occurs when $T \rightarrow 1$.

In Figs. 5(c) and 5(d), we compare the error probability of target detection when the quantum entanglement is maximized for the three different NGOCMs. From Fig. 5(c), we can see that for the case of double-side operations, the double-side PA operation gives the lowest error probability for a given number of copies K . This is because the double-side PA

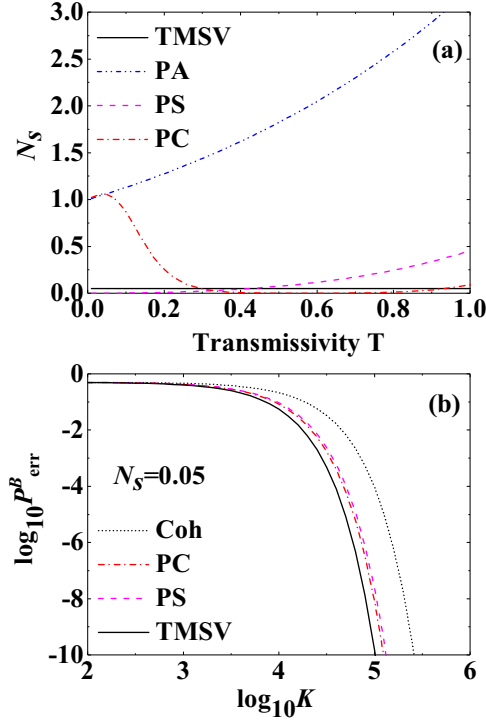


FIG. 4. (a) The average photon numbers of the signal source as a function of transmissivity for performing the PC operations (red line with circles), the PS operations (magenta line with diamonds), and the PA operations (blue line with triangles) on the initial entanglement source. The signal intensity of the TMSV is also shown as a benchmark for performance comparison (black lines). The squeezing parameter of the incident TMSV source is fixed to be $\sinh^2(r) = 0.05$. (b) For a given $N_s = 0.05$, the error probability as a function of number of copies K by performing the PC and PS operations on the initial TMSV source. The error probability of the TMSV (black solid line) and coherent state (black dotted line) are also shown as benchmark for comparison. The reflectivity of the target is chosen as $\kappa = 0.01$. The thermal noise intensity is $N_e = 1$.

operation increases both the entanglement and the signal intensity of the entangled source, while the PS and PC operations do not significantly enhance signal intensity in the region where entanglement is improved (see Fig. 4). However, we should mention that increasing the signal intensity may also increase the exposure risk of the radar. Unlike double-side NGOCMs, Fig. 5(d) shows that performing single-sided PC on the entangled source at the maximum entanglement can achieve the lowest error probability of target detection. Therefore, for single-sided NGOCMs, PC operation on the entangled source is preferred to reduce the error probability of target detection.

B. Signal-to-noise ratio for the homodyne detection as receiver

In this subsection, we consider to use homodyne detection (HD) instead of POVM for implementing the joint quantum measurement on the return and idler lights, as shown in Fig. 6. First, the returned and idler light are injected into the 50:50 optical beam splitter (BS_1), and the input-output relationship

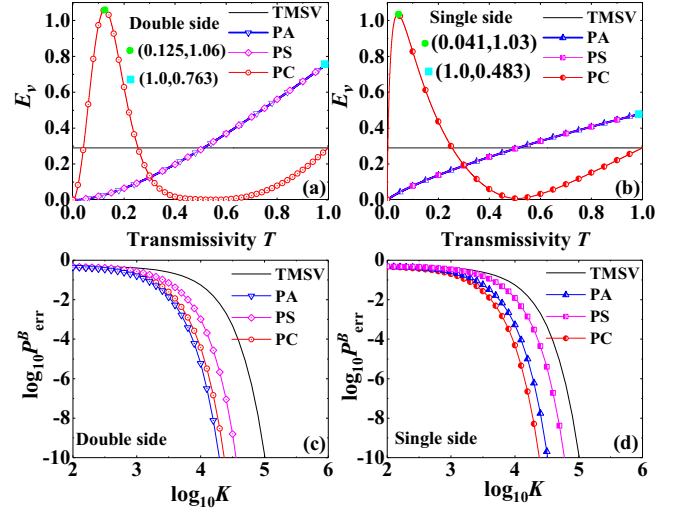


FIG. 5. Upper panel: The von Neumann entropy E_v as a function of transmissivity T of the NGOCMs for (a) the double-side NGOCMs and (b) the single-side NGOCMs. Lower panel: The error probability of the target detection as a function of number of copies K for (c) the double-side NGOCMs and (d) the single-side NGOCMs by taking the points with the maximum entanglement in (a) and (b). The reflectivity of the target is chosen as $\kappa = 0.01$. The squeezing parameter of the incident TMSV source is fixed to be $\sinh^2(r) = 0.05$ and the thermal noise intensity is $N_e = 1$.

can be represented as

$$\begin{pmatrix} \hat{b}_1 \\ \hat{b}_2 \end{pmatrix} = \frac{1}{\sqrt{2}} \begin{pmatrix} 1 & 1 \\ -1 & 1 \end{pmatrix} \begin{pmatrix} \hat{a}_R \\ \hat{a}_I \end{pmatrix}, \quad (10)$$

where \hat{b}_1 and \hat{b}_2 correspond to the annihilation operators of the two outputs of BS_1 . Then we implement the HD on each of the two output fields, respectively. The HD can be described as an

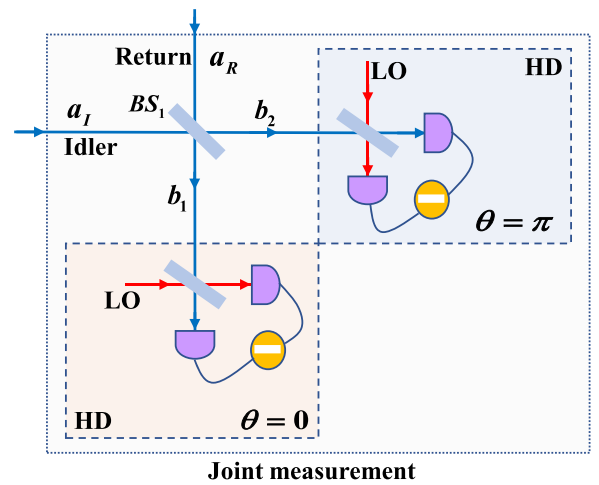


FIG. 6. A schematic diagram of the joint quantum measurement by homodyne detection. A return and idler beam are injected into 50:50 beam splitter (BS_1), and then the HD are performed on each output port of the beam splitter. In the mode b_1 , HD on the position quadrature ($\theta = 0$) is performed, and HD on the momentum quadrature ($\theta = \pi/2$) is performed in the mode b_2 .

input signal and a local oscillator (LO) being injected into a 50:50 beam splitter. Then, we measure the intensity difference between the output ports repeatedly [51]. In general, the LO is a strong laser beam whose amplitude and phase can be easily modulated. The measurement operator of the HD can be defined as

$$\hat{X}_j = \frac{\hat{b}_j^\dagger e^{i\theta_j} + \hat{b}_j e^{-i\theta_j}}{\sqrt{2}} \quad (j = 1, 2). \quad (11)$$

By modulating the phase θ_j of the LO, we can measure the position quadrature in mode b_1 when $\theta_1 = 0$ and the momentum quadrature in mode b_2 when $\theta_2 = \pi/2$. Here we employ TMSV as a benchmark to identify the advantages of non-Gaussian states, but the expectation value of its quadrature operator is always zero. To avoid this, we use the squared outcomes of the HD, i.e., $\hat{A} = [\hat{X}_1(0)]^2 + [\hat{X}_2(\pi/2)]^2$. Using Eqs. (10) and (11), we can obtain the effective operator for the joint quantum measurement given by

$$\hat{A} = \hat{a}_R \hat{a}_R^\dagger - \hat{a}_R^\dagger \hat{a}_I^\dagger - \hat{a}_R \hat{a}_I + \hat{a}_I^\dagger \hat{a}_I. \quad (12)$$

We anticipate that the enhancement of entanglement can result in an increase in the signal-to-noise ratio (SNR), consequently reducing the error probability in target detection for this specific detection method. By utilizing the measurement operator in Eq. (12) to measure the return and idle light, we can determine its expected value

$$M_x = \text{Tr}(\hat{A} \rho_{\text{SI}}^{(x)}), \quad (13)$$

and the variance

$$\Delta M_x = \text{Tr}(\hat{A}^2 \rho_{\text{SI}}^{(x)}) - [\text{Tr}(\hat{A} \rho_{\text{SI}}^{(x)})]^2, \quad (14)$$

where $\rho_{\text{SI}}^{(x)}$ denotes the density matrix without ($x = 0$) or with ($x = 1$) target information. Direct detection of all K return-idler copies, the SNR is given by

$$\text{SNR}(\text{dB}) = 10 \log_{10} \left[\frac{K(M_0 - M_1)^2}{2(\sqrt{\Delta M_0} + \sqrt{\Delta M_1})^2} \right] (\text{dB}). \quad (15)$$

Figure 7(a) shows the SNRs as a function of the target reflectivity κ for a given $K = 10^6$ when performing the PC operation on the TMSV. The SNR of the TMSV QI is plotted as a benchmark (black line). We can observe an obvious improvement in the SNR at the parameters $T = 0.1$ and 0.2 . Especially, when $T = 0.1$, the SNR can be enhanced by about ~ 6.4 dB for most values of κ . As expected, when the reflectivity κ decreases to zero, the SNR also decreases to zero.

To further illustrate the advantages of non-Gaussian strategies, in Fig. 7(b), we show the SNR as a function of the number of copies K for a fixed $\kappa = 0.01$ when implementing the PC operation on the TMSV. We can observe that by performing the PC operations on the entangled source, using fewer copies (K) can achieve similar SNR as that of the TMSV. For instance, for obtaining about 20 dB of the SNR, the number of copies required for the PC-TMSV source is much less than that of the TMSV (about $\Delta K = K_{\text{TMSV}} - K_{\text{PC-TMSV}} \approx 1.3 \times 10^6$ for $T = 0.1$ and $\Delta K = K_{\text{TMSV}} - K_{\text{PC-TMSV}} \approx 1.05 \times 10^6$ for $T = 0.2$).

Finally, we compare the SNR for three different NGOCMs. In Fig. 8 we present the SNR as a function of κ for different double-side NGOCMs with their maximum entanglement

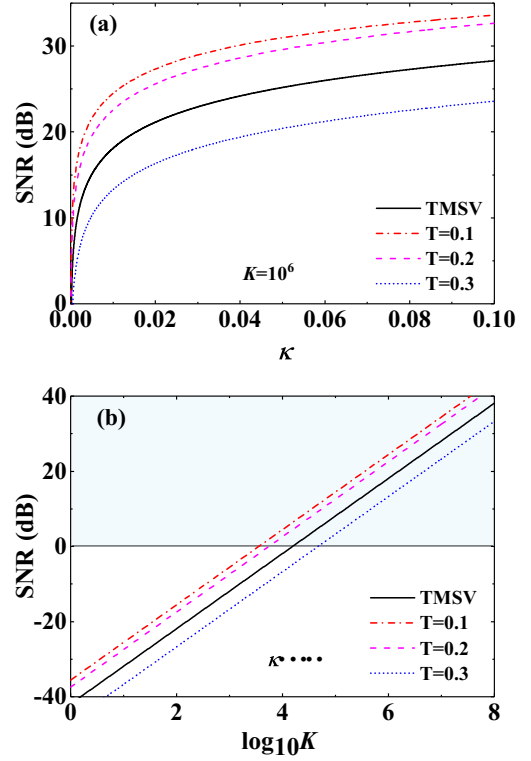


FIG. 7. The SNR as a function of (a) reflectivity κ of the target for a given $K = 10^6$ and (b) the number of copies K for a given $\kappa = 0.01$ when performing the PC operators with $T = (0.1, 0.2, 0.3)$ on the TMSV. The SNR of the TMSV is also shown as a benchmark for performance comparison (black lines). The squeezing parameter of the incident TMSV source is fixed to be $\sinh^2(r) = 0.05$ and the thermal noise intensity is $N_e = 1$.

point ($T_{\text{PC}} = 0.125$ for the PC operation and $T_{\text{PA}} = T_{\text{PS}} = 1$ for the PA and PS operations). For comparison, the SNR of the TMSV scheme is also depicted (black line). It is evident that all NGOCMs can substantially enhance the SNR of target

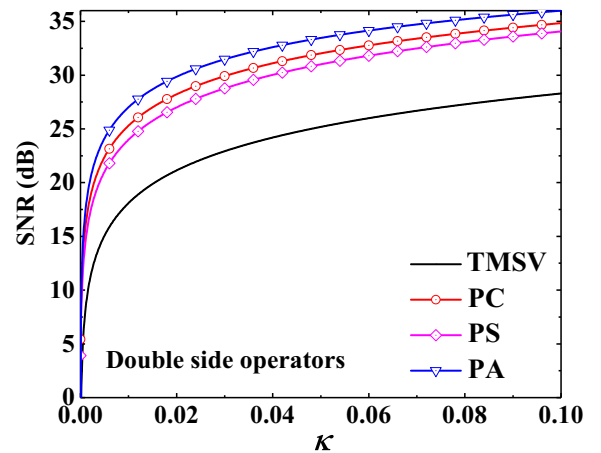


FIG. 8. The SNR as a function of reflectivity κ of the target for different double-side NGOCMs in their maximum entanglement points. The squeezing parameter of the incident TMSV source is fixed to be $\sinh^2(r) = 0.05$ and the thermal noise intensity is $N_e = 1$.

detection compared with that of the usual TMSV. Among the three types of NGOCMs, the PA operation exhibits the largest enhancement, i.e., enhancing the SNR by about 9 dB. The PS operation can improve the SNR by about 6 dB.

IV. CONCLUSION

In summary, we propose to perform single-photon non-Gaussian operations based on conditional measurements (NGOCM) on the Gaussian entangled state and employ them as radiation sources to illuminate an unknown target concealed within background noise. We explore the enhancement of quantum illumination performance achieved by these NGOCMs, which include single-photon addition, subtraction, and catalysis. Our research indicates that the error probability of target detection can be significantly reduced by modulating the initial entangled state using these NGOCMs. In addition to the enhancement of quantum entanglement, PA operation can further reduce the detection error probability by increasing the signal intensity which is a classical effect. In addition, our results show that with the same average signal photon number, the entangled light source such as TMSV, PS- and PC-TMSV can produce smaller error probability than that using the coherent state and the TMSV gives the smallest error rate.

In addition, we consider balanced homodyne detection as a specific joint quantum measurement scheme. In this scheme, performing the single-photon addition operation on a Gaussian entangled source can increase the signal-to-noise ratio (SNR) of target detection by 9 dB compared with that using the TMSV as entanglement source. Although single-photon subtraction operation has the least improvement, it can still improve the SNR by 6 dB. Our results here can find applications in the quantum illumination and similar non-Gaussian quantum operations may be able to achieve quantum enhancement for target localization and velocity detection as well which will be studied in the future.

ACKNOWLEDGMENTS

This work was supported by the National Key R&D Program of China (Grant No. 2021YFA1400800), the Key Program of National Natural Science Foundation of China (Grant No. 12334017), and the Natural Science Foundations of Guangdong (Grant No. 2021A1515010039).

APPENDIX: DERIVATION OF THE NORMALIZED COEFFICIENTS c_n OF THE NON-GAUSSIAN STATES IN EQ. (2)

As shown in Fig. 9, an m -photon ancillary Fock state in mode c is incident on one of the input ports of beam splitter with reflectivity $T = \cos^2 \theta$, and then the corresponding output of the interference is measured on Fock state with n photon at one of the output ports. Mathematically, for any quantum state $|\psi\rangle_{in}$ as another input port of the beam splitter, we can get $|\psi\rangle_{out} \rightarrow \hat{O}_{kl}|\psi\rangle_{in}$, where \hat{O}_{kl} can be expressed as

$$\hat{O}_{kl} = \langle l|B(T)|k\rangle, \quad (A1)$$

where $B(T) = \exp\{\arccos \sqrt{T}(c^\dagger S - cS^\dagger)\}$ is the beam-splitter operator. In the coherent state representation of Fock

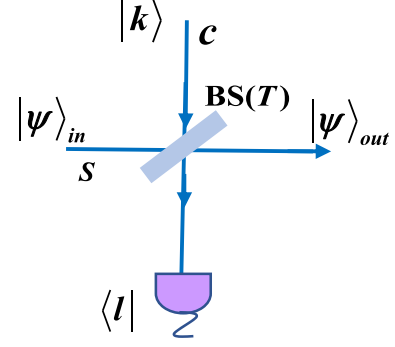


FIG. 9. Schematic setup of the non-Gaussian operations. An input state $|\psi\rangle_{in}$ and a Fock state $|k\rangle$ are present in the two input ports of the BS. Measurement is conditioned on registering an l -photon Fock $|l\rangle$.

state, the normally ordering form of $B(T)$ can be rewritten as [52]

$$B(T) =: \exp\{(\sqrt{T}-1)(c^\dagger c + S^\dagger S) + (S^\dagger c - Sc^\dagger)\sqrt{1-T}\}, \quad (A2)$$

where the symbol $:x:$ denotes the normal ordering of operators. By using the formulas $|k\rangle = \frac{1}{\sqrt{k!}} \frac{\partial^k}{\partial \alpha^k} \exp(\alpha c^\dagger)|0\rangle|_{\alpha=0}$ in an un-normalized coherent state representation [53], we can obtain

$$\hat{O}_{kl} = \frac{(-\sqrt{T})^k}{\sqrt{k!l!}} : H_{k,l} \left(S^\dagger \sqrt{\frac{1-T}{T}}, S \sqrt{\frac{1-T}{T}} \right) : e^{S^\dagger S \ln \sqrt{T}}, \quad (A3)$$

where $H_{k,l}(x,y) = \frac{\partial^{k+l}}{\partial u^k \partial v^l} \exp[-uv + ux + vy]|_{u=v=0}$ is the generating function of two-variable Hermite polynomials [54]. In particular, when $k=1$ and $l=0$, we can obtain the PS operation, i.e.,

$$\hat{O}_{PS} = \sqrt{\frac{1-T}{T}} S e^{S^\dagger S \ln \sqrt{T}}. \quad (A4)$$

Applying the PS operator [Eq. (A4)] to the two modes of the TMSV state [Eq. (1)], we can obtain the PS-TMSV state [Eq. (2)] with

$$c_{n,PS} = \sqrt{\frac{(1-\lambda^2 T^4)^3}{(1+\lambda^2 T^4)}} (n+1) \lambda^n T^{2n}. \quad (A5)$$

It should be noted that here we set the symmetrical double-side PS operation, i.e., the transmissivity $T_1 = T_2 = T$ of the optical beam splitters. When $k=0$ and $l=1$, we can get the PA operation, i.e.,

$$\hat{O}_{PA} = -\sqrt{1-T} S^\dagger e^{S^\dagger S \ln \sqrt{T}}. \quad (A6)$$

Furthermore, we can obtain the PA-TMSV state with

$$c_{n,PA} = \sqrt{\frac{(1-\lambda^2 T^4)^3}{(1+\lambda^2 T^4)}} n \lambda^{n-1} T^{2(n-1)}. \quad (A7)$$

When $k = l = 1$, we can obtain the PC operation, i.e.,

$$\hat{O}_{\text{PC}} = \sqrt{T} : \frac{1-T}{T} S^\dagger S - 1 : e^{S^\dagger S \ln \sqrt{T}}. \quad (\text{A8})$$

Same method as obtaining Eqs. (A5) and (A6), applying the PC operator to the two modes of the TMSV state [Eq. (1)], we can obtain the PC-TMSV state with

$$c_{n,\text{PC}} = \frac{1}{\sqrt{N}} \lambda^n T^{2(n-1)} [T^2 - n(1-T^2)]^2, \quad (\text{A9})$$

where

$$N^{-2} = \frac{1-\lambda^2}{(1-\lambda^2 T^4)^5} [T^4 + (1-8T^2+24T^4-32T^6+11T^8) \times \lambda^2 + T^4(11-56T^2+96T^4-56T^6+11T^8)\lambda^4 + T^4(11-32T^2+24T^4-8T^6+T^8)\lambda^6 + T^{12}\lambda^8]. \quad (\text{A10})$$

-
- [1] T. Albash and D. A. Lidar, Adiabatic quantum computation, *Rev. Mod. Phys.* **90**, 015002 (2018).
 - [2] R. Raussendorf and H. J. Briegel, A one-way quantum computer, *Phys. Rev. Lett.* **86**, 5188 (2001).
 - [3] H. J. Briegel, D. E. Browne, W. Dür, R. Raussendorf, and M. Van den Nest, Measurement-based quantum computation, *Nat. Phys.* **5**, 19 (2009).
 - [4] S. L. Braunstein and P. van Loock, Quantum information with continuous variables, *Rev. Mod. Phys.* **77**, 513 (2005).
 - [5] N. Gisin and R. Thew, Quantum communication, *Nat. Photonics* **1**, 165 (2007).
 - [6] X. Y. Lu, Q. Li, D. A. Westly, G. Moille, A. Singh, V. Anant, and K. Srinivasan, Chip-integrated visible–telecom entangled photon pair source for quantum communication, *Nat. Phys.* **15**, 373 (2019).
 - [7] C. L. Degen, F. Reinhard, and P. Cappellaro, Quantum sensing, *Rev. Mod. Phys.* **89**, 035002 (2017).
 - [8] S. Pirandola, B. R. Bardhan, T. Gehring, C. Weedbrook, and S. Lloyd, Advances in photonic quantum sensing, *Nat. Photonics* **12**, 724 (2018).
 - [9] M. Tsang, R. Nair, and X.-M. Lu, Quantum theory of superresolution for two incoherent optical point sources, *Phys. Rev. X* **6**, 031033 (2016).
 - [10] H. Zhang, W. Ye, C. Wei, Y. Xia, S. Chang, Z. Liao, and L. Hu, Improved phase sensitivity in a quantum optical interferometer based on multiphoton catalytic two-mode squeezed vacuum states, *Phys. Rev. A* **103**, 013705 (2021).
 - [11] S. Lloyd, Enhanced sensitivity of photodetection via quantum illumination, *Science* **321**, 1463 (2008).
 - [12] S. H. Tan, B. I. Erkmen, V. Giovannetti, S. Guha, S. Lloyd, L. Maccone, S. Pirandola, and J. H. Shapiro, Quantum illumination with Gaussian states, *Phys. Rev. Lett.* **101**, 253601 (2008).
 - [13] L. Maccone and C. L. Ren, Quantum radar, *Phys. Rev. Lett.* **124**, 200503 (2020).
 - [14] Q. T. Zhuang and J. H. Shapiro, Ultimate accuracy limit of quantum pulse-compression ranging, *Phys. Rev. Lett.* **128**, 010501 (2022).
 - [15] K. M. R. Audenaert, J. Calsamiglia, R. Muñoz-Tapia, E. Bagan, L. Masanes, A. Acín, and F. Verstraete, Discriminating states: The quantum Chernoff bound, *Phys. Rev. Lett.* **98**, 160501 (2007).
 - [16] J. Calsamiglia, R. Muñoz-Tapia, L. Masanes, A. Acín, and E. Bagan, Quantum Chernoff bound as a measure of distinguishability between density matrices: Application to qubit and Gaussian states, *Phys. Rev. A* **77**, 032311 (2008).
 - [17] J. H. Shapiro, The quantum illumination story, *IEEE Aerosp. Electron. Syst. Mag.* **35**, 8 (2020).
 - [18] M. Sanz, U. Las Heras, J. J. García-Ripoll, E. Solano, and R. Di Candia, Quantum estimation methods for quantum illumination, *Phys. Rev. Lett.* **118**, 070803 (2017).
 - [19] F. X. Xu, X. M. Zhang, L. Xu, T. Jiang, M. H. Yung, and L. J. Zhang, Experimental quantum target detection approaching the fundamental helstrom limit, *Phys. Rev. Lett.* **127**, 040504 (2021).
 - [20] M. H. Yung, F. Meng, X. M. Zhang, and M. J. Zhao, One-shot detection limits of quantum illumination with discrete signals, *npj Quantum Inf.* **6**, 75 (2020).
 - [21] E. D. Lopaeva, I. Ruo Berchera, I. P. Degiovanni, S. Olivares, G. Brida, and M. Genovese, Experimental realization of quantum illumination, *Phys. Rev. Lett.* **110**, 153603 (2013).
 - [22] Z. S. Zhang, S. Mouradian, F. N. C. Wong, and J. H. Shapiro, Entanglement-enhanced sensing in a lossy and noisy environment, *Phys. Rev. Lett.* **114**, 110506 (2015).
 - [23] Q. T. Zhuang, Z. T. Zhang, and J. H. Shapiro, Optimum mixed-state discrimination for noisy entanglement-enhanced sensing, *Phys. Rev. Lett.* **118**, 040801 (2017).
 - [24] M. Bradshaw, L. O. Conlon, S. Tserkis, M. Gu, P. K. Lam, and S. M. Assad, Optimal probes for continuous-variable quantum illumination, *Phys. Rev. A* **103**, 062413 (2021).
 - [25] B. H. Wu, S. Guha, and Q. T. Zhuang, Entanglement-assisted multi-aperture pulse-compression radar for angle resolving detection, *Quantum Sci. Technol.* **8**, 035016 (2023).
 - [26] R. Gallego Torromé, Quantum illumination with multiple entangled photons, *Adv. Quantum Technol.* **4**, 2100101 (2021).
 - [27] S. L. Zhang, J. S. Guo, W. S. Bao, J. H. Shi, C. H. Jin, X. B. Zou, and G. C. Guo, Quantum illumination with photon-subtracted continuous-variable entanglement, *Phys. Rev. A* **89**, 062309 (2014).
 - [28] L. F. Fan and M. S. Zubairy, Quantum illumination using non-Gaussian states generated by photon subtraction and photon addition, *Phys. Rev. A* **98**, 012319 (2018).
 - [29] T. J. Bartley, G. Donati, J. B. Spring, X. M. Jin, M. Barbieri, A. Datta, B. J. Smith, and I. A. Walmsley, Multiphoton state engineering by heralded interference between single photons and coherent states, *Phys. Rev. A* **86**, 043820 (2012).
 - [30] M. Walschaers, Non-Gaussian quantum states and where to find them, *PRX Quantum* **2**, 030204 (2021).
 - [31] S. Grebien, J. Götttsch, B. Hage, J. Fiuřášek, and R. Schnabel, Multistep two-copy distillation of squeezed states via two-photon subtraction, *Phys. Rev. Lett.* **129**, 273604 (2022).
 - [32] N. Namekata, Y. Takahashi, G. Fujii, D. Fukuda, S. Kurimura, and S. Inoue, Non-Gaussian operation based on photon subtraction using a photon-number-resolving detector at a telecommunications wavelength, *Nat. Photonics* **4**, 655 (2010).

- [33] H. Takahashi, J. S. Neergaard-Nielsen, M. Takeuchi, M. Takeoka, K. Hayasaka, A. Furusawa, and M. Sasaki, Entanglement distillation from Gaussian input states, *Nat. Photonics* **4**, 178 (2010).
- [34] S. Liu, D. Han, N. Wang, Y. Xiang, F. Sun, M. Wang, Z. Qin, Q. Gong, X. Su, and Q. He, Experimental demonstration of remotely creating wigner negativity via quantum steering, *Phys. Rev. Lett.* **128**, 200401 (2022).
- [35] A. E. Ulanov, I. A. Fedorov, A. A. Pushkina, Y. V. Kurochkin, T. C. Ralph, and A. Lvovsky, Undoing the effect of loss on quantum entanglement, *Nat. Photonics* **9**, 764 (2015).
- [36] W. Ye, H. Zhong, Q. Liao, D. Huang, L. Hu, and Y. Guo, Improvement of self-referenced continuous-variable quantum key distribution with quantum photon catalysis, *Opt. Express* **27**, 17186 (2019).
- [37] L. Hu, M. Al-amri, Z. Liao, and M. S. Zubairy, Continuous-variable quantum key distribution with non-Gaussian operations, *Phys. Rev. A* **102**, 012608 (2020).
- [38] D. Braun, P. Jian, O. Pinel, and N. Treps, Precision measurements with photon-subtracted or photon-added Gaussian states, *Phys. Rev. A* **90**, 013821 (2014).
- [39] H. Zhang, W. Ye, S. K. Chang, Y. Xia, L. Y. Hu, and Z. Y. Liao, Quantum multiparameter estimation with multi-mode photon catalysis entangled squeezed state, *Front. Phys.* **18**, 42304 (2023).
- [40] Y. Yang and F. L. Li, Entanglement properties of non-Gaussian resources generated via photon subtraction and addition and continuous-variable quantum-teleportation improvement, *Phys. Rev. A* **80**, 022315 (2009).
- [41] A. Zavatta, S. Viciani, and M. Bellini, Quantum-to-classical transition with single-photon-added coherent states of light, *Science* **306**, 660 (2004).
- [42] X. X. Xu, Enhancing quantum entanglement and quantum teleportation for two-mode squeezed vacuum state by local quantum-optical catalysis, *Phys. Rev. A* **92**, 012318 (2015).
- [43] T. J. Bartley and I. A. Walmsley, Directly comparing entanglement-enhancing non-Gaussian operations, *New J. Phys.* **17**, 023038 (2015).
- [44] Y.-S. Ra, A. Dufour, M. Walschaers, C. Jacquard, T. Michel, C. Fabre, and N. Treps, Non-Gaussian quantum states of a multimode light field, *Nat. Phys.* **16**, 144 (2020).
- [45] F. Wong, J. Shapiro, and T. Kim, Efficient generation of polarization-entangled photons in a nonlinear crystal, *Laser Phys.* **16**, 1517 (2006).
- [46] M. Esposito, A. Ranadive, L. Planat, S. Leger, D. Fraudet, V. Jouanny, O. Buisson, W. Guichard, C. Naud, J. Aumentado *et al.*, Observation of two-mode squeezing in a traveling wave parametric amplifier, *Phys. Rev. Lett.* **128**, 153603 (2022).
- [47] C. H. Bennett, H. J. Bernstein, S. Popescu, and B. Schumacher, Concentrating partial entanglement by local operations, *Phys. Rev. A* **53**, 2046 (1996).
- [48] S. J. van Enk, Discrete formulation of teleportation of continuous variables, *Phys. Rev. A* **60**, 5095 (1999).
- [49] C. W. Helstrom, Quantum detection and estimation theory, *J. Stat. Phys.* **1**, 231 (1969).
- [50] S. Pirandola and S. Lloyd, Computable bounds for the discrimination of Gaussian states, *Phys. Rev. A* **78**, 012331 (2008).
- [51] S. L. Braunstein, Homodyne statistics, *Phys. Rev. A* **42**, 474 (1990).
- [52] H. Y. Fan, H. L. Lu, and Y. Fan, Newton–Leibniz integration for ket–bra operators in quantum mechanics and derivation of entangled state representations, *Ann. Phys.* **321**, 480 (2006).
- [53] L. Y. Hu, Z. Y. Liao, and M. S. Zubairy, Continuous-variable entanglement via multiphoton catalysis, *Phys. Rev. A* **95**, 012310 (2017).
- [54] A. Wünsche, General Hermite and Laguerre two-dimensional polynomials, *J. Phys. A: Math. Theor.* **33**, 1603 (2000).